

# Hygroscopic Properties of Internally Mixed Particles Composed of NaCl and Water-Soluble Organic Acids

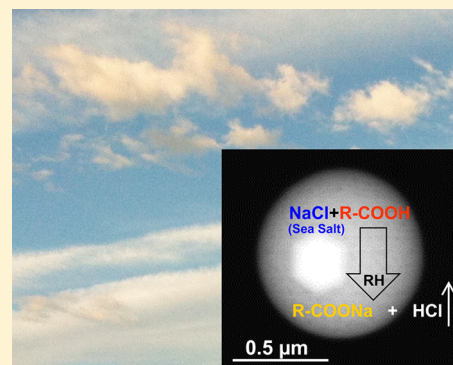
Suman Ghorai,<sup>†</sup> Bingbing Wang,<sup>‡</sup> Alexei Tivanski,<sup>\*,†</sup> and Alexander Laskin<sup>\*,‡</sup>

<sup>†</sup>Department of Chemistry, The University of Iowa, Iowa City, Iowa 52242, United States

<sup>‡</sup>William R. Wiley Environmental Molecular Sciences Laboratory, Pacific Northwest National Laboratory, Richland, Washington 99352, United States

**S** Supporting Information

**ABSTRACT:** Atmospheric aging of naturally emitted marine aerosol often leads to formation of internally mixed particles composed of sea salts and water-soluble organic compounds of anthropogenic origin. Mixing of sea salt and organic components has profound effects on the evolving chemical composition and hygroscopic properties of the resulted particles, which are poorly understood. Here, we have studied chemical composition and hygroscopic properties of laboratory generated NaCl particles mixed with malonic acid (MA) and glutaric acid (GA) at different molar ratios using micro-FTIR spectroscopy, atomic force microscopy, and X-ray elemental microanalysis. Hygroscopic properties of internally mixed NaCl and organic acid particles were distinctly different from pure components and varied significantly with the type and amount of organic compound present. Experimental results were in a good agreement with the AIM modeling calculations of gas/liquid/solid partitioning in studied systems. X-ray elemental microanalysis of particles showed that Cl/Na ratio decreased with increasing organic acid component in the particles with MA yielding lower ratios relative to GA. We attribute the depletion of chloride to the formation of sodium malonate and sodium glutarate salts resulted by HCl evaporation from dehydrating particles.



## INTRODUCTION

Atmospheric aerosol is a diverse mixture of externally and internally mixed particles containing various condensed phase compounds at different concentrations.<sup>1,2</sup> Compositional differences in these particles can create significant impacts on Earth's climate and the atmospheric environment.<sup>3,4</sup> For example, absorption and scattering of solar radiation, formation of cloud condensation nuclei, and heterogeneous reaction during their transport are all directly dependent on the chemical composition of the particles in the atmosphere.<sup>3–6</sup> Whereas many field and modeling studies tend to distinguish and separate environmental effects of organic and inorganic particles, complex aerosol particles with internally mixed inorganic and organic compounds are common in the atmosphere.<sup>7–11</sup> Inclusion of an organic component in an inorganic salt is particularly important as their physical properties tend to show a significant change in the mixture as compared to pure components.<sup>12</sup> Therefore, studies of both mixing states and compositional dependence of physical properties of the atmospheric particles are important for predictive understanding of their environmental effects.

One of the most important physical properties of atmospheric particles and of direct relevance to their radiative and cloud forming effects is their hygroscopicity.<sup>13,14</sup> The amount of water uptake by particle at a particular relative humidity (RH) depends on the overall chemical composition, mixing states and solubility of its components. For example,

recent studies have shown noticeable changes in hygroscopic properties of ammonium sulfate on internal mixing with organic acids.<sup>12,15</sup> Observed changes cannot be estimated in most cases based on linear combination of hygroscopic responses of the chemical components present. Several other examples with a mixture of different types of chemical components such as inorganic salts, organic substances, and several naturally occurring materials showed similarly significant effects on hygroscopic properties of complex aerosols that cannot be accounted by a combination of individual responses of components.<sup>15,16</sup> Moreover, prediction of water uptake using different environmental models has also been observed to fail for these complex mixtures.<sup>17</sup> The present study focuses on composition dependent hygroscopic properties of internally mixed NaCl/Malonic acid and NaCl/Glutaric acid particles.

Sea salt particles can react with atmospheric inorganic acids, such as nitric acid and sulfuric acid and form corresponding salts.<sup>18</sup> Furthermore, previous studies have reported a wide range of occurrence of malonic acid (MA) and glutaric acid (GA) in the atmosphere. The overall concentrations of atmospheric dicarboxylic acids (DCA) varies according to the meteorological conditions. A field study on samples collected

Received: October 22, 2013

Revised: January 9, 2014

Accepted: January 17, 2014

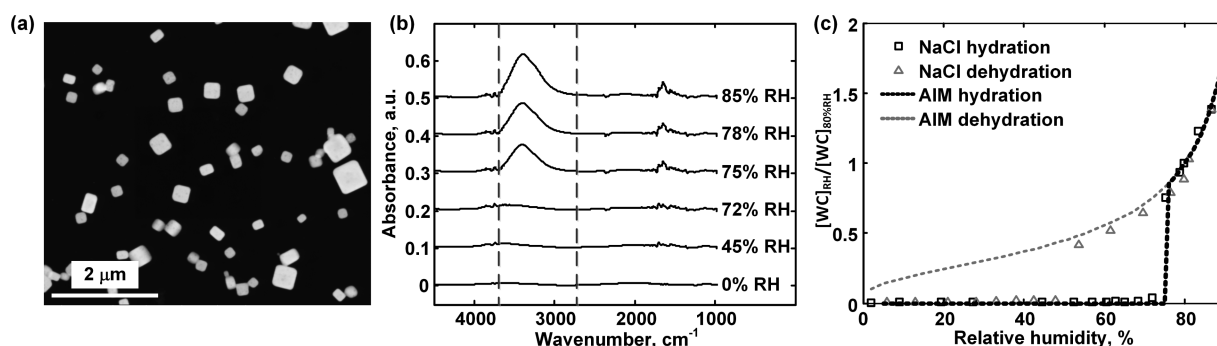
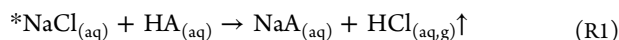


**Figure 1.** (a) SEM images (0% RH) of dry NaCl particles showing cubic shape of the crystals. (b) FTIR spectra of NaCl particles at selected RH showing appearance of broad  $-OH$  stretching band centered at  $\sim 3400\text{ cm}^{-1}$  as humidity increases. (c) Hydration and dehydration of NaCl particles quantified by plotting the ratio of peak area at a particular RH to that at 80% RH as a function of RH. Dotted lines represent the calculated response predicted by AIM model.

from Germany showed a typical concentration range of  $5\text{--}100\text{ ng m}^{-3}$  for low molecular weight DCA.<sup>19</sup> Other studies with samples from distinct places over the globe (Tokyo, Vienna and South Africa, Los Angeles, etc) showed DCA concentrations varying from a few  $\text{ng m}^{-3}$  to  $\mu\text{g m}^{-3}$  range.<sup>20,21</sup> We have recently observed a substantial reactivity of sea salt with organic acids in field samples collected in central California resulting in depletion of chloride in the particles.<sup>7</sup> The chloride depletion is a result of an acid displacement reaction R1, which is driven by high volatility of the HCl product.



Here,  $*\text{NaCl}$  represents a complex mixture of sea salt, and HA can be any organic or inorganic acid with low volatility. Because NaCl accounts for ca 90% of chloride in sea salt, we selected NaCl particles mixed with MA and GA as a laboratory system for our experiments. We show that the acid displacement can occur in the particles of internally mixed carboxylic acids with NaCl when particles go through the dehydration process. During the dehydration, the evaporation of HCl proceeds, resulting in compositional changes (depletion of chloride and formation of organic sodium salt) of these internally mixed NaCl/organic acid particles.<sup>7</sup> Previous studies on the mixture of MA and GA with NaCl demonstrated the effect of organic acids on NaCl hygroscopic properties.<sup>16,22</sup> A study by Choi et al. on hygroscopic properties of mixture of glutaric and malonic acid with NaCl showed that the resulting water uptake by these mixture samples cannot be accurately predicted using modeling approach based on the ZSR mixing rules and the water activity of individual components.<sup>18</sup> Another study, by Pope et al., showed a slightly different effect compared to the study by Choi et al. with similar glutaric and malonic acid mixture with NaCl.<sup>22</sup> In this study, X-ray elemental analysis of individual particles was used to determine the composition of NaCl particles mixed with MA and GA for better understanding of these largely neglected reactions between organic acids and NaCl. Micro-FTIR was used to determine the water content in reacted particles as a function of RH, and to investigate the effects of these reactions on particle hygroscopicity.

## EXPERIMENTAL DETAILS

All samples of submicrometer sized particles were generated using constant output atomizer (TSI, Inc., model 3076) from aqueous 0.2 M solution prepared from reagent-plus-grade chemicals (99.99% purity, Aldrich). The solution was prepared

with deionized water ( $18\text{ M}\Omega\text{-cm}$ ). Aerosol was dried down to  $\sim 30\%$  RH in a diffusion dryer (TSI, Inc., model 3062) prior to sizing and collection using a micro-orifice uniform deposit impactor (MOUDI) (MSP, Inc., model 110). Particles were deposited on  $\text{Si}_3\text{N}_4$  windows (Silson Ltd., England) and TEM grids (Carbon Type-B, Ted Pella, Inc.) mounted on the impaction plate of the seventh stage of the MOUDI. The aerodynamic cutoff size of the seventh stage was  $0.32\text{ }\mu\text{m}$ . Samples collected on  $\text{Si}_3\text{N}_4$  windows and TEM grids were used for micro-FTIR<sup>23</sup> and computer controlled scanning electron microscopy with energy dispersed analysis of X-ray (CCSEM/EDX)<sup>24</sup> analysis, respectively. All samples were prepared at room temperature and used within a couple of days after the preparation.

A detailed description of the micro-FTIR experiment and its application for studies of hygroscopic properties has been reported elsewhere,<sup>25,26</sup> and thus will be described only briefly here. In this setup, a Bruker A590 IR optical microscope is interfaced with a Bruker IFS 66/S FTIR spectrometer equipped with a liquid-nitrogen-cooled mercury–cadmium–telluride (MCT) detector. Cassegrainian optics were used to focus the IR beam on the sample and to collect the transmitted IR light after its interaction with the sample. The  $\text{Si}_3\text{N}_4$  substrate with deposited particles was placed in a sample holder inside a sealed environmental stage (model THMS 600, Linkam, Inc.). RH inside the environmental stage was controlled by a continuous flow of mixed dry and humidified nitrogen with a total flow rate of 1.0 slpm. An inline humidity sensor (Honeywell, Inc., model HIH4000) was used to monitor RH with an uncertainty of 3% at room temperature. FTIR absorbance spectra were acquired by coadding 512 scans at a resolution of  $4\text{ cm}^{-1}$ . A typical equilibration time of 5 min was used for measurement at each RH. An ensemble of approximately 100 particles deposited on the substrate was monitored in each of the hydration/dehydration experiments. Condensed-phase water in the particles was quantified from the integrated absorbance of the OH stretching band.<sup>25</sup>

Due to residual charging issue in SEM for the pure organic acid particles, atomic force microscopy (AFM) was used in addition to SEM to obtain particle morphology for some of the samples. AFM has been used to obtain 3D height images of substrate-deposited MA and GA particles. AFM images were obtained using molecular force probe 3D AFM (Asylum Research, Santa Barbara, CA). Height images were collected using intermittent contact mode (AC mode) at room temperature using silicon probes (MikroMasch, San Jose, CA,

CSC37) with a nominal spring constant of  $0.35 \text{ N m}^{-1}$  and a typical tip radius of curvature of 10 nm.

A FEG XL30 scanning electron microscope (FEI, Inc.) was used to investigate the morphology and elemental composition of individual particles. The microscope is equipped with an X-ray spectrometer (EDAX, Inc.) with a Si(Li) detector of an active area of  $30 \text{ mm}^2$  and an ATW2 window. The CCSEM/EDX analysis was performed in computer-controlled mode which provides the elemental composition of a statistically significant number of individual particles. Details of this instrument and its applications for particle analysis are published elsewhere.<sup>24</sup>

## RESULTS AND DISCUSSION

Previous studies have shown that NaCl particles exhibit distinct water uptake with deliquescence relative humidity (DRH) and efflorescence relative humidity (ERH) at 75% and 48%, respectively.<sup>27–36</sup> On the other hand, dicarboxylic acids such as MA and GA show continuous water uptake as a function of RH without sharp deliquescence or efflorescence phase transitions.<sup>16</sup> In this study, we show that internally mixing MA and GA with NaCl in various molar ratios results in drastic changes in water uptake properties of NaCl, studied by micro-FTIR spectroscopy. The chloride to sodium (Cl/Na) ratios of individual particles from the CCSEM/EDX analysis are used to identify the interactions between organic acids and NaCl and provide possible reason behind changes in hygroscopic properties of NaCl when mixed with MA and GA at different molar ratios.

Figure 1a shows the SEM images of NaCl submicrometer particles with characteristic morphology of cubic crystals.<sup>25</sup> Figure 1b shows the FTIR spectra acquired for an ensemble of these particles at increasing RH. Initially, no distinct signature in the FTIR spectra was observed. When RH is gradually increased, a new peak due to the OH stretching band of the condensed water grows in the region from  $3660$  to  $2750 \text{ cm}^{-1}$  (indicated by the dashed lines in Figure 1b) and its integrated peak area is used to quantify the hygroscopic properties.<sup>25,37</sup>

With a stepwise increase in RH, absorption spectra were continuously recorded (only selected spectra are shown here). NaCl particles deliquesce at around 75% RH, resulting in an abrupt increase in the absorbance in the peak centered at  $3400$  and  $1640 \text{ cm}^{-1}$ .<sup>25</sup> The water content in NaCl deliquesced droplets continues to grow with further increase in RH as indicated by –OH band growth and expansion. Infrared spectra of the NaCl droplets recorded in the dehydration cycle (not shown here) are similar to those in Figure 1b and an abrupt decrease in the water band absorption at ~48% RH confirmed efflorescence phase transition. Both deliquescence and efflorescence RH values of pure NaCl particles are in good agreement with the literature.<sup>38</sup>

The change in water content within the particle throughout the complete hydration/dehydration cycle is shown in Figure 1c. The relative particle water content (WC) defined as  $[\text{WC}]_{\text{RH}}/[\text{WC}]_{80\% \text{RH}} = A_{\text{RH}}/A_{80\% \text{RH}}$ , is expressed by plotting the integrated peak area ( $A_{\text{RH}}$ , between  $3660$  and  $2750 \text{ cm}^{-1}$ ) normalized to the integrated peak area at 80% RH ( $A_{80\% \text{RH}}$ ) as a function of RH. The uncertainty associated with the determination of WC is ca 3–4%. Our measurement is also compared with the prediction of water uptake by AIM aerosol thermodynamic model (Model III)<sup>39</sup> and expressed as the same  $[\text{WC}]_{\text{RH}}/[\text{WC}]_{80\% \text{RH}}$  relative values. The calculated dehydration curves for all the samples have been generated by allowing

the components to exist in a metastable liquid state (i.e., formation of solid phases was disabled in the model input). The hygroscopic properties of NaCl particles observed here are consistent with the literature and AIM model.<sup>25,40,41</sup>

Water uptake of the pure MA and GA particles were recorded next. AFM images were acquired initially to characterize the morphology of the deposited particles. Figure 2 shows an AFM height image of dry MA and GA particles.

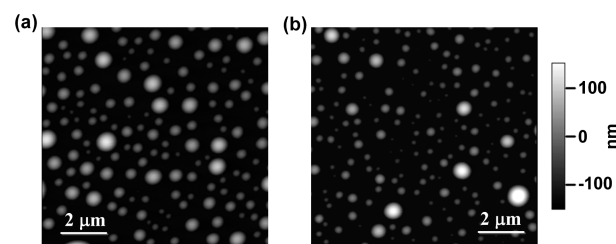


**Figure 2.** Representative AFM height images (~30% RH) of (a) MA and (b) GA particles with sizes ranging between  $0.2$  and  $1.2 \mu\text{m}$ .

Particle size has been measured to be in the range of  $0.2$ – $1.2 \mu\text{m}$  for both the samples. The droplet-like, spherical particle morphology is consistent with reported work on MA and GA particles in the literature.<sup>37,42</sup> FTIR spectra of MA and GA particles acquired at different RH settings in the environmental stage are shown in Figure 3a,b, respectively. Typical IR absorption bands of the organic acids were observed in the beginning of the experiment at 2% RH, with nearly undetectable amount of water. All relevant IR features of dry MA and GA were verified with literature and reported in Table 1.<sup>42–45</sup> The transition centered at  $\sim 3000 \text{ cm}^{-1}$  (Figure 3a,b) interferes with the water peak at  $\sim 3400 \text{ cm}^{-1}$ . Therefore, IR spectrum at ~2% RH was subtracted from all the IR spectra at higher RH to remove spectral features that originate from organic acids toward particle water content measurements. Moreover, peak broadening and peak shifts in the IR spectra of MA and GA particles were observed, a typical phenomenon reported in our previous water uptake studies of MA and others in the literature.<sup>23,37</sup>

With gradual increase in RH, particle water content increases and the characteristic –OH stretching band due to adsorbed water was observed, centered at  $\sim 3400 \text{ cm}^{-1}$ . The relative water content in MA and GA particles have been measured as  $[\text{WC}]_{\text{RH}}/[\text{WC}]_{80\% \text{RH}} = A_{\text{RH}}/A_{80\% \text{RH}}$  ratio in the identical way as the NaCl particles and compared with the prediction by the AIM model.<sup>46,47</sup> Figure 3c shows the  $[\text{WC}]_{\text{RH}}/[\text{WC}]_{80\% \text{RH}}$  ratios in hydration/dehydration experiments with MA particles. The prediction by the AIM model (fitted activity equation used in the parametrization) and our experimental results are in good agreement with each other. Comparison of hygroscopic properties of GA particles (Figure 3d) with the AIM model showed slight under estimation of the modeled values above deliquescence, which was observed at the RH predicted by the model. Overall, the water uptake by the pure organic acids measured in this work was consistent with the AIM thermodynamic model. However, unlike NaCl particles, MA and GA particles did not exhibit well-defined deliquescence and efflorescence phase transitions. Although MA particles showed nearly continuous water uptake, GA particles have a poorly defined deliquescence transition at ~80% RH. No clear efflorescence was observed for either of the samples. Shape of the hygroscopic curves and absence of sharp phase transition

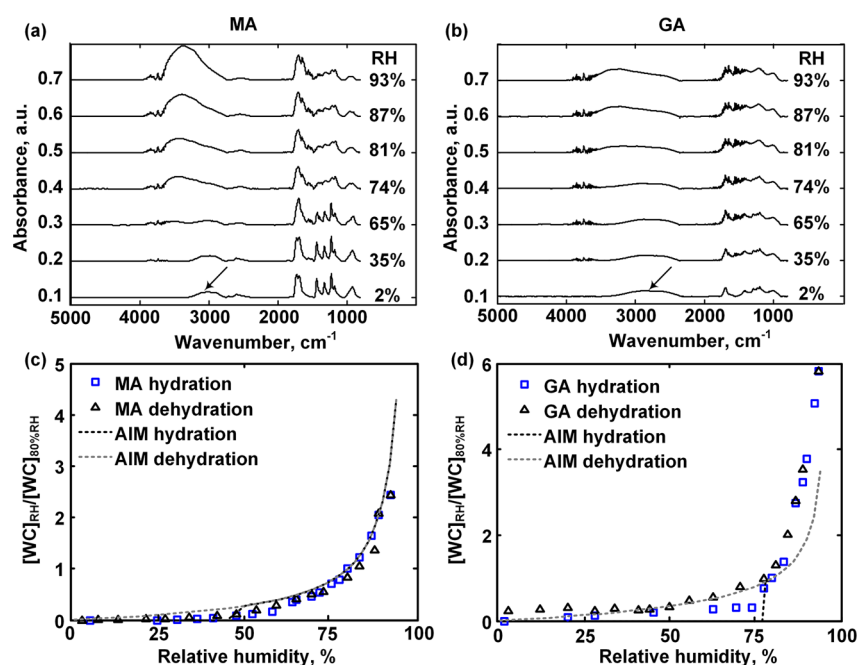


**Figure 3.** Changes in FTIR spectra of MA (a) and GA (b) particles as a function of RH. The gradual increase in  $-\text{OH}$  stretch in the spectral region of  $2750\text{--}3660\text{ cm}^{-1}$  was similar to the NaCl particles. Relative water content in MA (c) and GA (d) particles compared with the AIM model prediction.

**Table 1.** FTIR Peak Assignment of Malonic Acid (MA) and Glutaric Acid (GA)

compound	absorption maxima, $\text{cm}^{-1}$	assignment
malonic acid <sup>31–33</sup>	1174	$\gamma(\text{CH}_2)$ , $\omega(\text{CH}_2)$
	1223	$\gamma(\text{C}=\text{C})$
	1323	$\gamma(\text{C}=\text{O})$
	1431	$\nu(\text{O}=\text{H})$ , $\delta(\text{CH}_2)$
	1722	$\nu(\text{C}=\text{O})$
glutaric acid <sup>30</sup>	1200	$\gamma(\text{CH}_2)$
	1238	$\omega(\text{CH}_2)$ , $\gamma(\text{C}=\text{C})$
	1294	$\nu(\text{C}=\text{O})$
	1414	$\nu(\text{O}=\text{H})$ , $\delta(\text{CH}_2)$
	1697	$\nu(\text{C}=\text{O})$

\*Bands are as shown in Figure 3a, b.  $\nu$ , stretching;  $\omega$ , bending;  $\gamma$ , rocking.

for dicarboxylic acid components are consistent with the literature.<sup>37,48,49</sup>

Next, internally mixed MA/NaCl and GA/NaCl particles were studied. Figure 4 shows morphology of the internally mixed dry MA/NaCl and GA/NaCl particles that varied significantly, depending on the mixing ratios. Whereas NaCl particles were cubic in shape (Figure 1a), the mixed particles had more rounded morphology. For both mixtures, increase in the relative amount of organic acid transformed the particle morphology toward more spherical in shape. Differences have been also observed between morphologies of MA/NaCl and GA/NaCl particles at the same molar ratio. For example, as shown in Figure 4a,d, particles at a 1:3 molar ratio are more rectangular-shaped for GA/NaCl as compared to MA/NaCl mixtures. Notable inhomogeneous mixing states were observed for the most of the samples, such as a core–shell structure (1:1 MA/NaCl, Figure 4b), and inclusion of small sodium chloride crystals within overall spherical particles (3:1 GA/NaCl, Figure 4f). Interestingly, MA/NaCl particles at a 3:1 mixing ratio

(Figure 4c) were seen as homogeneous spherical particles, whereas GA/NaCl particles at the same mixing ratio (Figure 4f) showed observable inhomogeneity in their visual appearance. Overall, addition of MA to NaCl had a greater impact on the particle morphology and vanishing of NaCl crystalline inclusions as compared to GA.

In aqueous micrometer size droplets, MA and GA can react with NaCl through acid displacement reactions releasing gas-phase HCl and forming sodium malonate and sodium glutarate in the particle phase:  $\text{NaCl}_{(\text{aq})} + \text{MA}_{(\text{aq})}$  ( $\text{GA}_{(\text{aq})}$ )  $\rightleftharpoons$  sodium malonate<sub>(aq)</sub> (sodium glutarate<sub>(aq)</sub>) +  $\text{HCl}_{(\text{aq}, \text{g})}$ . Hence, particle samples were subjected to CCSEM elemental analysis, expecting the chloride depletion resulted from evaporation of HCl.<sup>7</sup> Effects of particle size on the Cl depletion has been evaluated based on the analysis of more than 1500 individual particles in each sample. The particle size distribution for each sample is shown in Figure S1 (Supporting Information). Figure 5 shows the mean elemental Cl/Na ratio as a function of particle size. For pure NaCl particles, experimentally determined Cl/Na ratios match their nominal value of 1 for micrometer-size particles and then deviate toward lower 0.9 value for smaller particles because of the beam damage of particles. Nevertheless, observed Cl/Na values were used as a reference to evaluate extent of the Cl depletion in mixed MA/NaCl and GA/NaCl particles. GA/NaCl particles with 1:3 and 1:1 molar ratios showed only minor Cl depletion, as evidenced by a small decrease in Cl/Na ratios. At a higher ratio of 3:1, GA/NaCl particles showed 20–30% of Cl depletion. In contrast, the MA/NaCl particles displayed substantially greater levels of Cl depletion, as high as 10–20%, 30–40%, and 100% for 1:3, 1:1 and 3:1 mixtures, respectively.

Chloride depletion in mixed MA/NaCl and GA/NaCl particles results in formation of corresponding sodium salts (sodium malonate and sodium glutarate) that become a significant component of these particles. Although these reactions are not thermodynamically favored in bulk solutions,

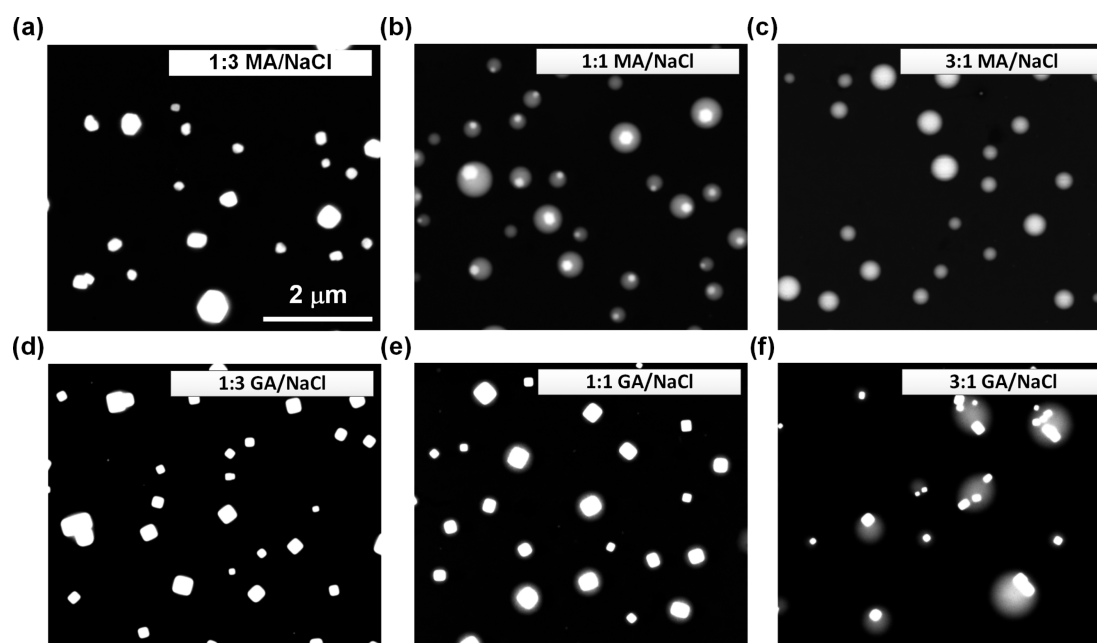


**Figure 4.** SEM images of dry particles (0% RH) showing morphology of MA/NaCl and GA/NaCl particles prepared from solutions with different molar ratios.

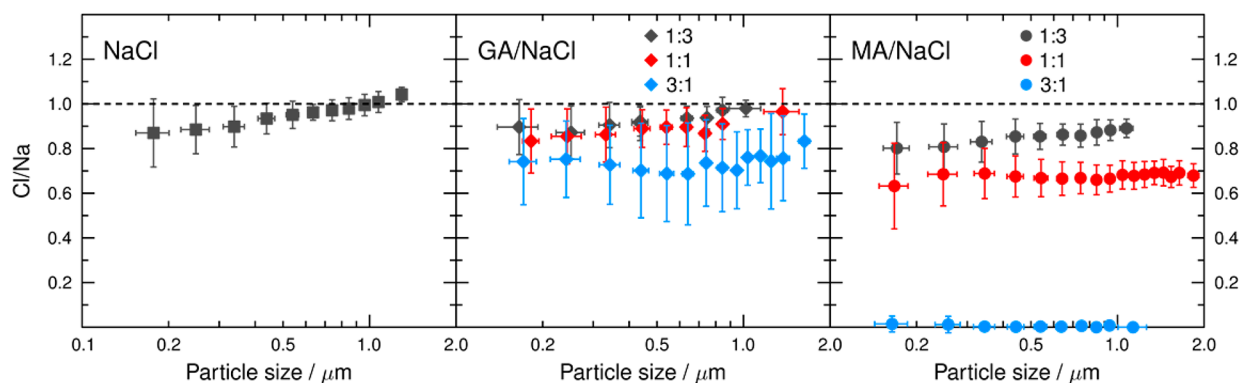


**Figure 5.** Mean elemental Cl/Na ratio as a function of particle size for NaCl, GA/NaCl and MA/NaCl particles with different molar ratios. Dash lines indicate nominal value of Cl/Na = 1 in pure NaCl particles. Error bars indicate a standard deviation of 1.

**Table 2. Composition of Dry NaCl/MA and NaCl/GA Particles Generated from Solution**

mixing ratio in solution			composition of dry particles (molar percentage, %)					
NaCl	MA	GA	Cl/Na	NaCl	MA	GA	sodium malonate	sodium glutarate
3	1		$0.85 \pm 0.1$	$72 \pm 3$	$15 \pm 7$		$13 \pm 10$	
1	1		$0.7 \pm 0.1$	$41 \pm 3$	$41 \pm 3$		$18 \pm 7$	
1	3		0	0	67		33	
3		1	1	75		25		0
1		1	$0.95 \pm 0.1$	$49 \pm 3$		$49 \pm 3$		$3 \pm 3$
1		3	$0.7 \pm 0.2$	$19 \pm 6$		$73 \pm 3$		$8 \pm 6$

irreversible evaporation of HCl gas is the main driving force for this type of reaction that likely took place when atomized aerosol was introduced in the diffusion dryer during sample preparation.<sup>7</sup> Enrichment of particles in sodium malonate and sodium glutonate salts can be quantified from measured Cl/Na ratios and the resulting chemical composition of particles in all studied samples is tabulated in Table 2, whereas SEM images of Figure 4 illustrate corresponding changes in the particle morphology. It is worthwhile to mention that complete Cl depletion in MA/NaCl particles at the mixing ratio of 3:1

(Figure 4c) indicates effective transformation of their chemical composition to that of the MA/sodium malonate mixtures (free of NaCl) that form homogeneous rounded particles. Following the observed changes in morphology and Cl depletion due to HCl evaporation, we performed hydration/dehydration experiments with the internally mixed particles to probe effects of this chemistry on water uptake.

Figure 6 shows the relative water content in the mixed particles measured as  $[WC]_{RH}/[WC]_{80\%RH} = A_{RH}/A_{80\%RH}$  ratio for all six samples. In contrast to NaCl particles, the abrupt

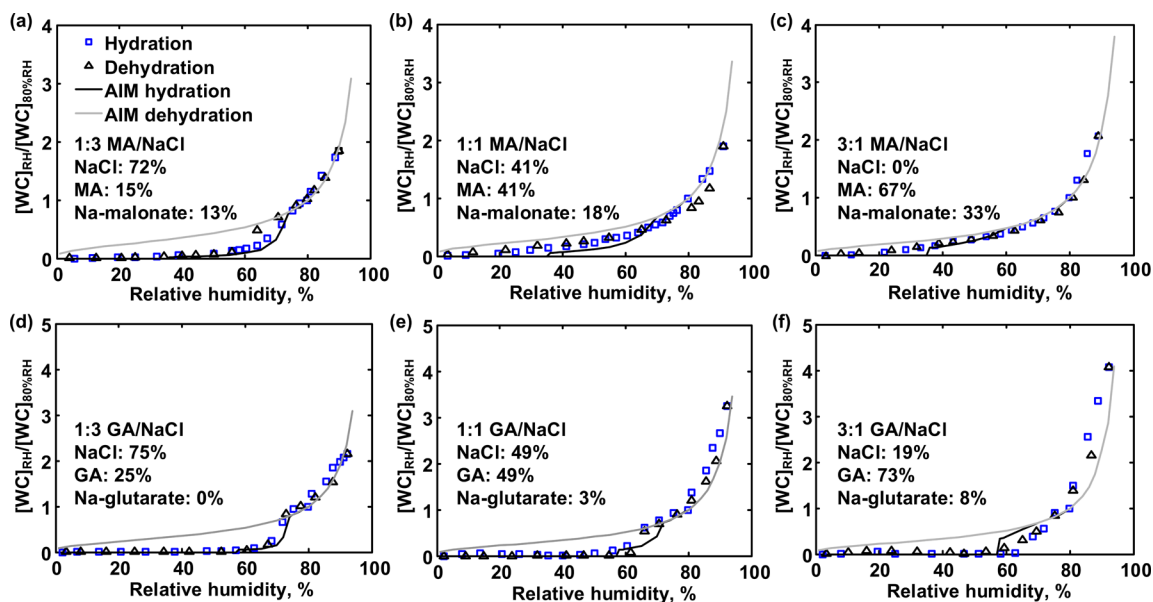


**Figure 6.** Relative water content in internally mixed MA/NaCl (a, b, c) and GA/NaCl (d, e, f) particles with different molar ratios. The solid lines represent the AIM calculation. Experimental data for mixed MA/NaCl particles showed a better overall match with the AIM model prediction.

deliquescence and efflorescence phase transitions were not observed for any of these samples. For the 1:3 mixed MA/NaCl particles (Figure 6a) the deliquescence transition took place over a broad range of 55–75% RH, and the hysteresis between the hydration and the dehydration cycles was also diminished. With increased amounts of MA at 1:1 and 3:1 ratios in MA/NaCl particles (Figures 6b,c), the hydration curves showed continuous water uptake starting from below 50% RH. These observations are somewhat different from hygroscopic behavior of larger (5–10  $\mu\text{m}$ ) particles of mixed MA/NaCl (1:1) studied previously by Choi and Chen in electrodynamic balance experiment,<sup>16</sup> where deliquescence and efflorescence phase transition were still distinct. It is plausible that submicrometer particles probed in our experiment may stay metastable (liquid-like) over wide range of RH, exhibiting gradual water uptake/evaporation in the hydration/dehydration cycle.

In the case of GA/NaCl particles with the 1:3 ratio (Figure 6d), deliquescence phase transition plodded over a range of 65–75% RH, without hysteresis between hydration and dehydration curves. Relative to the GA/NaCl particles with the 1:3 ratio, the 1:1 and 3:1 GA/NaCl mixed particles (Figure 6e,f) showed greater effect on the vanishing of deliquescence and transforming the hygroscopic properties of particles to more continuous water uptake as a function of RH. Notably, no major differences were observed between hydration and dehydration experiments for all mixed particle samples studied here, including those cases where deliquescence and efflorescence transitions were clearly observed (Figure 6a,d,e). It can be argued that this might be an effect of substrate–particle interactions that promote efflorescence phase transitions for substrate deposited particles that possibly would have taken place at substantially lower RH if the particles were levitated. Although these possible effects of substrates cannot be completely ruled out, our similar experiments<sup>23,27</sup> with substrate deposited NaCl, sea salt,  $\text{NaNO}_3$ , and  $(\text{NH}_4)_2\text{SO}_4$  particles always showed dehydration curves consistent with those reported in the literature for levitated particles.<sup>38</sup>

Solid lines in the plots of Figure 6 show relative water content of particles calculated at different RH using the AIM

model for hydration (black lines) and dehydration (gray lines) experiments.<sup>46,47</sup> The dehydration curves were calculated for supersaturated metastable particles where precipitation of the solid phases was disabled in the model input. Presently, the AIM model does not consider formation of either sodium malonic or sodium glutaric salts, and includes only water activity of the organic acids themselves for calculating solid/liquid/gas partitioning in aerosol. This limitation does not allow model calculations with the correct composition of MA/NaCl and GA/NaCl particles as listed in Table 2 for this study. Instead, the relative water content is calculated for particles with the nominal MA(GA)/NaCl composition prior to the reactions between their components and the evaporation of HCl. Comparison of the modeling results with our experimental measurements indicates that the formation of the sodium organic salts would have only marginal influence on the overall hydration properties of mixed particles studied here, and their liquid water content can be reasonably estimated by the AIM model, assuming nominal (unreacted) composition of the MA(GA)/NaCl mixed particles. This moderate match between the AIM calculations and the experimental data is likely indicative of close similarities between hygroscopic properties of MA(GA) and their corresponding Na-salts.

However, composition of the reacted NaCl/MA(GA) particles and especially internal heterogeneity of these particles may have important consequences on particle acidity, optical properties, viscosity, dynamics of phase separations, and reactivity with gas-phase species. Presently, these changes in particle properties are not considered in the interpretation of neither experimental data from field or laboratory studies, nor they are assumed by any of the atmospheric modeling studies. Results of our study warrant additional tests to probe these potential ramifications of the sea salt–organic acid chemistry in the atmospheric environment.

## ■ ASSOCIATED CONTENT

### Supporting Information

Size distributions in reported particle samples and method to calculate the Cl/Na atomic ratios in particle samples reported

in Table 2. This material is available free of charge via the Internet at <http://pubs.acs.org>.

## AUTHOR INFORMATION

### Corresponding Authors

\*Alexei Tivanski. Phone: (319)-384-3692. Fax: (319)-335-1270. E-mail: [alexei-tivanski@uiowa.edu](mailto:alexei-tivanski@uiowa.edu).

\*Alexander Laskin. Phone: (509)-371-6129. Fax: (509)-371-6139. E-mail: [alexander.laskin@pnnl.gov](mailto:alexander.laskin@pnnl.gov).

### Notes

The authors declare no competing financial interest.

## ACKNOWLEDGMENTS

S.G. and A.V.T. gratefully acknowledge financial support from the National Oceanic and Atmospheric Administration (NOAA) Climate Program Office, Earth System Science Program, award NA11OAR4310187. S.G. acknowledges additional sponsorship provided by the 2009 Summer Research Institute on Interfacial and Condensed Phase Chemical Physics organized at PNNL. B.W. and A.L. acknowledge support by the Laboratory Directed Research and Development funds of Pacific Northwest National Laboratory (PNNL) through the Chemical Imaging Initiative. The micro-FTIR and CCSEM experiments were performed at the William R. Wiley Environmental Molecular Sciences Laboratory, a national scientific user facility sponsored by the DOE's Office of Biological and Environmental Research and located at PNNL. Pacific Northwest National Laboratory is operated for the U.S. Department of Energy by Battelle Memorial Institute under Contract No. DE-AC06-76RLO 1830. We thank P. L. Gassman and J. P. Cain for assistance with the micro-FTIR instrument.

## REFERENCES

- (1) Pöschl, U. Atmospheric aerosols: Composition, transformation, climate and health effects. *Angew. Chem., Int. Ed.* **2005**, *44*, 7520–7540.
- (2) Prather, K. A.; Hatch, C. D.; Grassian, V. H. Analysis of atmospheric aerosols. *Annu. Rev. Anal. Chem.* **2008**, *1*, 485–514.
- (3) Cwiertny, D. M.; Young, M. A.; Grassian, V. H. Chemistry and photochemistry of mineral dust aerosol. *Annu. Rev. Phys. Chem.* **2008**, *59*, 27–51.
- (4) Hanke, M.; Umann, B.; Uecker, J.; Arnold, F.; Bunz, H. Atmospheric measurements of gas-phase HNO<sub>3</sub> and SO<sub>2</sub> using chemical ionization mass spectrometry during the MINATROC field campaign 2000 on Monte Cimone. *Atmos. Chem. Phys.* **2003**, *3*, 417–436.
- (5) Ramanathan, V.; Crutzen, P. J.; Kiehl, J. T.; Rosenfeld, D. Atmosphere—Aerosols, climate, and the hydrological cycle. *Science* **2001**, *294*, 2119–2124.
- (6) Usher, C. R.; Al-Hosney, H.; Carlos-Cuellar, S.; Grassian, V. H. A laboratory study of the heterogeneous uptake and oxidation of sulfur dioxide on mineral dust particles. *J. Geophys. Res. Atmos.* **2002**, *107* (D23), 4713 DOI: 10.1029/2002JD002051.
- (7) Laskin, A.; Moffet, R. C.; Gilles, M. K.; Fast, J. D.; Zaveri, R. A.; Wang, B.; Nigge, P.; Shuttanandan, J. Tropospheric chemistry of internally mixed sea salt and organic particles: Surprising reactivity of NaCl with weak organic acids. *J. Geophys. Res. Atmos.* **2012**, *117*, D15302 DOI: 10.1029/2012JD017743.
- (8) Qin, X.; Pratt, K. A.; Shields, L. G.; Toner, S. M.; Prather, K. A. Seasonal comparisons of single-particle chemical mixing state in Riverside, CA. *Atmos. Environ.* **2012**, *59*, 587–596.
- (9) Hiranuma, N.; Brooks, S. D.; Moffet, R. C.; Glen, A.; Laskin, A.; Gilles, M. K.; Liu, P.; Macdonald, A. M.; Strapp, J. W.; McFarquhar, G. M. Chemical characterization of individual particles and residuals of cloud droplets and ice crystals collected on board research aircraft in the ISDAC 2008 study. *J. Geophys. Res. Atmos.* **2013**, *118*, 6564–6579.
- (10) Moffet, R. C.; Furutani, H.; Rodel, T. C.; Henn, T. R.; Sprau, P. O.; Laskin, A.; Uematsu, M.; Gilles, M. K. Iron speciation and mixing in single aerosol particles from the Asian continental outflow. *J. Geophys. Res. Atmos.* **2012**, *117*, D07204/1–D07204/12, DOI: 10.1029/2011JD016746.
- (11) Zardini, A. A.; Sjogren, S.; Marcolli, C.; Krieger, U. K.; Gysel, M.; Weingartner, E.; Baltensperger, U.; Peter, T. A combined particle trap/HTDMA hygroscopicity study of mixed inorganic/organic aerosol particles. *Atmos. Chem. Phys.* **2008**, *8*, 5589–5601.
- (12) Yeung, M. C.; Chan, C. K. Water content and phase transitions in particles of inorganic and organic species and their mixtures using micro-Raman spectroscopy. *Aerosol. Sci. Tech.* **2010**, *44*, 269–280.
- (13) Michel Flores, J.; Bar-Or, R. Z.; Bluvshstein, N.; Abo-Riziq, A.; Kostinski, A.; Borrmann, S.; Koren, I.; Rudich, Y. Absorbing aerosols at high relative humidity: linking hygroscopic growth to optical properties. *Atmos. Chem. Phys.* **2012**, *12*, 5511–5521.
- (14) Gysel, M.; Weingartner, E.; Nyeki, S.; Paulsen, D.; Baltensperger, U.; Galambos, I.; Kiss, G. Hygroscopic properties of water-soluble matter and humic-like organics in atmospheric fine aerosol. *Atmos. Chem. Phys.* **2004**, *4*, 35–50.
- (15) Shi, Y.; Ge, M.; Wang, W. Hygroscopicity of internally mixed aerosol particles containing benzoic acid and inorganic salts. *Atmos. Environ.* **2012**, *60*, 9–17.
- (16) Choi, M. Y.; Chan, C. K. The effects of organic species on the hygroscopic behaviors of inorganic aerosols. *Environ. Sci. Technol.* **2002**, *36*, 2422–2428.
- (17) Attwood, A. R.; Greenslade, M. E. Deliquescence behavior of internally mixed clay and salt aerosols by optical extinction measurements. *J. Phys. Chem. A* **2012**, *116*, 4518–4527.
- (18) ten Brink, H. M. Reactive uptake of HNO<sub>3</sub> and H<sub>2</sub>SO<sub>4</sub> in sea-salt (NaCl) particles. *J. Aerosol Sci.* **1998**, *29*, 57–64.
- (19) Grosjean, D.; van Cauwenberghe, K.; Schmid, J.; Kelley, P.; Pitts, J. N. Identification of C3-C10 aliphatic dicarboxylic acids in airborne particulate matter. *Environ. Sci. Technol.* **1978**, *12*, 313–317.
- (20) Sempère, R.; Kawamura, K. Comparative distributions of dicarboxylic acids and related polar compounds in snow, rain and aerosols from urban atmosphere. *Atmos. Environ.* **1994**, *28*, 449–459.
- (21) Limbeck, A.; Puxbaum, H. Organic acids in continental background aerosols. *Atmos. Environ.* **1999**, *33*, 1847–1852.
- (22) Pope, F. D.; Dennis-Smith, B. J.; Griffiths, P. T.; Clegg, S. L.; Cox, R. A. Studies of single aerosol particles containing malonic acid, glutaric acid, and their mixtures with sodium chloride. I. Hygroscopic growth. *J. Phys. Chem. A* **2010**, *114*, 5335–5341.
- (23) Liu, Y.; Yang, Z.; Desyaterik, Y.; Gassman, P. L.; Wang, H.; Laskin, A. Hygroscopic behavior of substrate-deposited particles studied by micro-FT-IR spectroscopy and complementary methods of particle analysis. *Anal. Chem.* **2008**, *80*, 633–642.
- (24) Laskin, A.; Cowin, J. P.; Iedema, M. J. Analysis of individual environmental particles using modern methods of electron microscopy and X-ray microanalysis. *J. Electron Spectrosc. Relat. Phenom.* **2006**, *150*, 260–274.
- (25) Liu, Y.; Yang, Z. W.; Desyaterik, Y.; Gassman, P. L.; Wang, H.; Laskin, A.; Kim, S. J.; Han, J. Hygroscopic behavior of substrate-deposited particles studied by micro-FT-IR spectroscopy and complementary methods of particle analysis. *Anal. Chem.* **2008**, *80*, 7179–7179.
- (26) Liu, Y.; Laskin, A. Hygroscopic properties of CH<sub>3</sub>SO<sub>3</sub>Na, CH<sub>3</sub>SO<sub>3</sub>NH<sub>4</sub>, (CH<sub>3</sub>SO<sub>3</sub>)<sub>2</sub>Mg, and (CH<sub>3</sub>SO<sub>3</sub>)<sub>2</sub>Ca particles studied by micro-FTIR spectroscopy. *J. Phys. Chem. A* **2009**, *113*, 1531–1538.
- (27) Ghorai, S.; Tivanski, A. V. Hygroscopic behavior of individual submicrometer particles studied by X-ray spectromicroscopy. *Anal. Chem.* **2010**, *82*, 9289–9298.
- (28) Cohen, M. D.; Flagan, R. C.; Seinfeld, J. H. Studies of concentrated electrolyte solutions using the electrodynamic balance. 1. Water activities for single-electrolyte solutions. *J. Phys. Chem.* **1987**, *91*, 4563–4574.
- (29) Cohen, M. D.; Flagan, R. C.; Seinfeld, J. H. Studies of concentrated electrolyte solutions using the electrodynamic balance. 2.

Water activities for mixed-electrolyte solutions. *J. Phys. Chem.* **1987**, *91*, 4583–4590.

(30) Cziczo, D. J.; Nowak, J. B.; Hu, J. H.; Abbatt, J. D. P. Infrared spectroscopy of model tropospheric aerosols as a function of relative humidity: Observation of deliquescence and crystallization. *J. Geophys. Res.* **1997**, *102*, 18843–18850.

(31) Cziczo, D. J.; Abbatt, J. P. D. Infrared observations of the response of NaCl, MgCl<sub>2</sub>, NH<sub>4</sub>HSO<sub>4</sub>, and NH<sub>4</sub>NO<sub>3</sub> aerosols to changes in relative humidity from 298 to 238 K. *J. Phys. Chem. A* **2000**, *104*, 2038–2047.

(32) Richardson, C. B.; Snyder, T. D. A study of heterogeneous nucleation in aqueous solutions. *Langmuir* **1994**, *10*, 2462–2465.

(33) Tang, I. N.; Munkelwitz, H. R. An investigation of solute nucleation in levitated solution droplets. *J. Colloid Interface Sci.* **1984**, *98*, 430–438.

(34) Tang, I. N.; Munkelwitz, H. R. Aerosol phase-transformation and growth in the atmosphere. *J. Appl. Meteorol.* **1994**, *33*, 791–796.

(35) Weis, D. D.; Ewing, G. E. Water content and morphology of sodium chloride aerosol particles. *J. Geophys. Res.* **1999**, *104*, 21275–21285.

(36) Wise, M. E.; Biskos, G.; Martin, S. T.; Russell, L. M.; Buseck, P. R. Aerosol phase transitions studied using a transmission electron microscope with an environmental cell. *Aerosol Sci. Technol.* **2005**, *39*, 849–856.

(37) Ghorai, S.; Laskin, A.; Tivanski, A. V. Spectroscopic evidence of keto-enol tautomerism in deliquesced malonic acid particles. *J. Phys. Chem. A* **2011**, *115*, 4373–4380.

(38) Martin, S. T. Phase transitions of aqueous atmospheric particles. *Chem. Rev.* **2000**, *100*, 3403–3454.

(39) Clegg, S. L.; Seinfeld, J. H. Thermodynamic models of aqueous solutions containing inorganic electrolytes and dicarboxylic acids at 298.15 K. 2. Systems including dissociation equilibria. *J. Phys. Chem. A* **2006**, *110*, 5718–5734.

(40) Hansson, H. C.; Rood, M. J.; Koloutsou-Vakakis, S.; Hameri, K.; Orsini, D.; Wiedensohler, A. NaCl aerosol particle hygroscopicity dependence on mixing with organic compounds. *J. Atmos. Chem.* **1998**, *31*, 321–346.

(41) Ma, Q. X.; Liu, Y. C.; He, H. The utilization of physisorption analyzer for studying the hygroscopic properties of atmospheric relevant particles. *J. Phys. Chem. A* **2010**, *114*, 4232–4237.

(42) Yeung, M. C.; Ling, T. Y.; Chan, C. K. Effects of the polymorphic transformation of glutaric acid particles on their deliquescence and hygroscopic properties. *J. Phys. Chem. A* **2010**, *114*, 898–903.

(43) Ganguly, S.; Fernandes, J. R.; Desiraju, G. R.; Rao, C. N. R. Phase-Transition in Malonic-Acid—Infrared Study. *Chem. Phys. Lett.* **1980**, *69*, 227–229.

(44) Li, L.; Dou, Q. Effects of malonic acid treatment on crystal structure, melting behavior, morphology, and mechanical properties of isotactic poly(propylene)/wollastonite composites. *Polym. Compos.* **2010**, *31*, 966–973.

(45) Macoas, E. M. S.; Fausto, R.; Lundell, J.; Pettersson, M.; Khriachtchev, L.; Rasanen, M. Conformational analysis and near-infrared-induced rotamerization of malonic acid in an argon matrix. *J. Phys. Chem. A* **2000**, *104*, 11725–11732.

(46) Clegg, S. L.; Brimblecombe, P.; Wexler, A. S. Thermodynamic model of the system H<sup>+</sup>–NH<sub>4</sub><sup>+</sup>–Na<sup>+</sup>–SO<sub>4</sub><sup>2-</sup>–NO<sub>3</sub><sup>-</sup>–Cl<sup>-</sup>–H<sub>2</sub>O at 298.15 K. *J. Phys. Chem. A* **1998**, *102*, 2155–2171.

(47) Clegg, S. L.; Brimblecombe, P.; Wexler, A. S. Thermodynamic model of the system H<sup>+</sup>–NH<sub>4</sub><sup>+</sup>–SO<sub>4</sub><sup>2-</sup>–NO<sub>3</sub><sup>-</sup>–H<sub>2</sub>O at tropospheric temperatures. *J. Phys. Chem. A* **1998**, *102*, 2137–2154.

(48) Peng, C.; Chan, M. N.; Chan, C. K. The hygroscopic properties of dicarboxylic and multifunctional acids: Measurements and UNIFAC predictions. *Environ. Sci. Technol.* **2001**, *35*, 4495–4501.

(49) Ling, T. Y.; Chan, C. K. Partial crystallization and deliquescence of particles containing ammonium sulfate and dicarboxylic acids. *J. Geophys. Res. Atmos.* **2008**, *113* (D14), D14205 DOI: 10.1029/2008JD009779.